Palaeogeography, Palaeoclimatology, Palaeoecology 510 (2018) 31–39

Contents lists available at ScienceDirect

Palaeogeography, Palaeoclimatology, Palaeoecology

journal homepage: www.elsevier.com/locate/palaeo

Orbital forcing of Plio-Pleistocene climate variation in a Qaidam Basin lake based on paleomagnetic and evaporite mineralogic analysis

Zeng Luo[a], Qingda Su[a], Zhao Wang[a], Richard V. Heermance[b], Carmala Garzione[c], Man Li[a], Xueping Ren[a], Yougui Song[d], Junsheng Nie[a,*]

[a] Key Laboratory of Western China's Environment System (Ministry of Education), College of Earth and Environmental Sciences, Lanzhou University, Lanzhou, Gansu 730000, China
[b] Department of Geological Sciences, California State University–Northridge, Northridge, California 91330-8266, USA
[c] Department of Earth and Environment Sciences, University of Rochester, Rochester, NY 14627, USA
[d] State Key Laboratory of Loess and Quaternary Geology, Institute of Earth Environment, Chinese Academy of Sciences, P.O. Box 17, Xi'an 710061, China

ARTICLE INFO

Keywords:
Aridification
Insolation forcing
Huatugou section
Eccentricity

ABSTRACT

Inland Asian aridification is threatening the global ecological system under continued global warming, requiring a full understanding of its forcing mechanisms. Past geological studies in this region focus mainly on initiation timing and million-year timescale variations in aridification. Few studies address the relationship between aridification and insolation forcing. Here we present a paleomagnetic and evaporite mineralogic study of the 476-m-long Huatugou (HTG) section (ca. 3.9 to 2.1 Ma) from the western Qaidam Basin. The results show that the drying of this part of the basin began by at least 3.9 Ma. Furthermore, we show that the relative content variation of evaporite minerals was dominated by 100-kyr cyclicity during the Pliocene. This is consistent with the result from the Xining area during the late Eocene. These results suggest that mid-latitude lacustrine evaporite minerals in semi-arid to arid regions are particularly sensitive to eccentricity forcing, improving understanding of aridification forcing at orbital timescales.

1. Introduction

More than 40% of the Earth's surface is being affected by aridification (Dregne et al., 1991; Wu et al., 2011; Feng and Fu, 2013). Among these arid areas, the drying of the Asian inland has attracted worldwide attention because of its threat to the ecological system and relevance to uplift of the Tibetan Plateau and retreat of the Paratethys. Over the past several decades, many aridification records with tectonic-timescale resolution have been generated and these results suggest that the drying of Asian inland began in the Miocene, or even late Oligocene (Sun et al., 1997; Song et al., 2001; An et al., 2001, 2006; Guo et al., 2002; Fang et al., 2007a; Song et al., 2007; D.H. Sun et al., 2008; J.M. Sun et al., 2008; Qiang et al., 2011; Song et al., 2013), intensified at the late Pliocene (~3.6 Ma) and early Pleistocene (~2.6 Ma) (Fang et al., 2008; Wu et al., 2011), and may be linked to the tectonic uplift of the Tibetan Plateau and global cooling (Ding et al., 1999; Guo et al., 2001; Hao and Guo, 2004; Fang et al., 2007b; Wu et al., 2007, 2011). However, at orbital-timescale, the relationship between the drying of Asian inland and insolation forcing is largely unknown because of the lack of well-dated high resolution paleoclimate records. As the main dust settling area, the orbital-timescale (10^4–10^5 yr) Asian aridification history can be potentially inferred from the Chinese Loess Plateau (CLP) records (Ding et al., 1994; Lu et al., 2004; Sun et al., 2006, 2010). Unfortunately, pre-Quaternary dust sedimentation rate of the CLP is so low that the orbital-timescale Asian aridification history is not well recorded (Lu et al., 2002, 2004). Thus, higher frequency changes in climate linked to insolation forcing is largely unknown prior to the Quaternary because of the lack of well-dated high resolution paleoclimate records. Moreover, recent studies reveal that the CLP dust does not necessarily come from inland Asian deserts, but instead, fluvial processes can contribute dust to the CLP (Stevens et al., 2013; Nie et al., 2014, 2015). To decipher the relationship between drying of the Asian inland and insolation forcing at orbital timescales, direct paleoclimate records from inland Asian basins are thus particularly important.

Evaporite minerals have proven to be a sensitive indicator of aridification (Fang et al., 1997; Williams-Stroud and Paul, 1997; Li et al., 2010, 2013). Evaporite minerals are abundant in inland continental basins, where carbonates, sulphates and chlorides precipitate within increasing drying of lake systems (Eugater and Hardie, 1978; Warren, 2006, 2010; Song et al., 2013; Zhang et al., 2013). Here we report

* Corresponding author.
E-mail address: jnie@lzu.edu.cn (J. Nie).

http://dx.doi.org/10.1016/j.palaeo.2017.09.022
Received 11 April 2017; Received in revised form 13 September 2017; Accepted 14 September 2017
Available online 21 September 2017
0031-0182/ © 2017 Elsevier B.V. All rights reserved.

records of evaporite mineral (halite, gypsum, carbonate) content records from the Huatugou (HTG) section in the western margin of the Qaidam Basin. These results provide a new, high-resolution record of climate change at the 10^5 yr scale that highlights the influence of insolation forcing on regional climate over the past 4 Myr.

2. Geologic setting

The Qaidam Basin, which is located within the northeastern corner of the Tibetan Plateau (Fig. 1A), is an inland intermontane basin that has existed since the Oligocene (Xia et al., 2001; Y.D. Wang et al., 2012; J.Y. Wang et al., 2012; Herb et al., 2015; Wang et al., 2017). It has a length of 850 km, a width of 250 km, and an area of 120,000 km^2 (Fang et al., 2008). It is bounded by the Kunlun Mts. to the south, the Altun Mts. to the northwest, the Qilian Mts. to the northeast, and the Ela Mts. to the east. Due to a relatively high elevation (about 2800–3100 masl) and surrounding ranges that block large amounts of water vapor, the interior of the basin has a cold and dry environment, with a mean annual temperature of 0–5 °C, average wind velocity 3.7–4.2 m/s, mean annual precipitation < 100 mm, and mean annual evaporation > 3000 mm (Zhang and Xuan, 1996; Li et al., 2010; Y.D. Wang et al., 2012; J.Y. Wang et al., 2012; Wang et al., 2013). Sparse desert vegetation, salt marshes, shifting sand and salt deposits cover much of the basin (Wu et al., 2011; Cai et al., 2012). Large amounts of Pliocene-

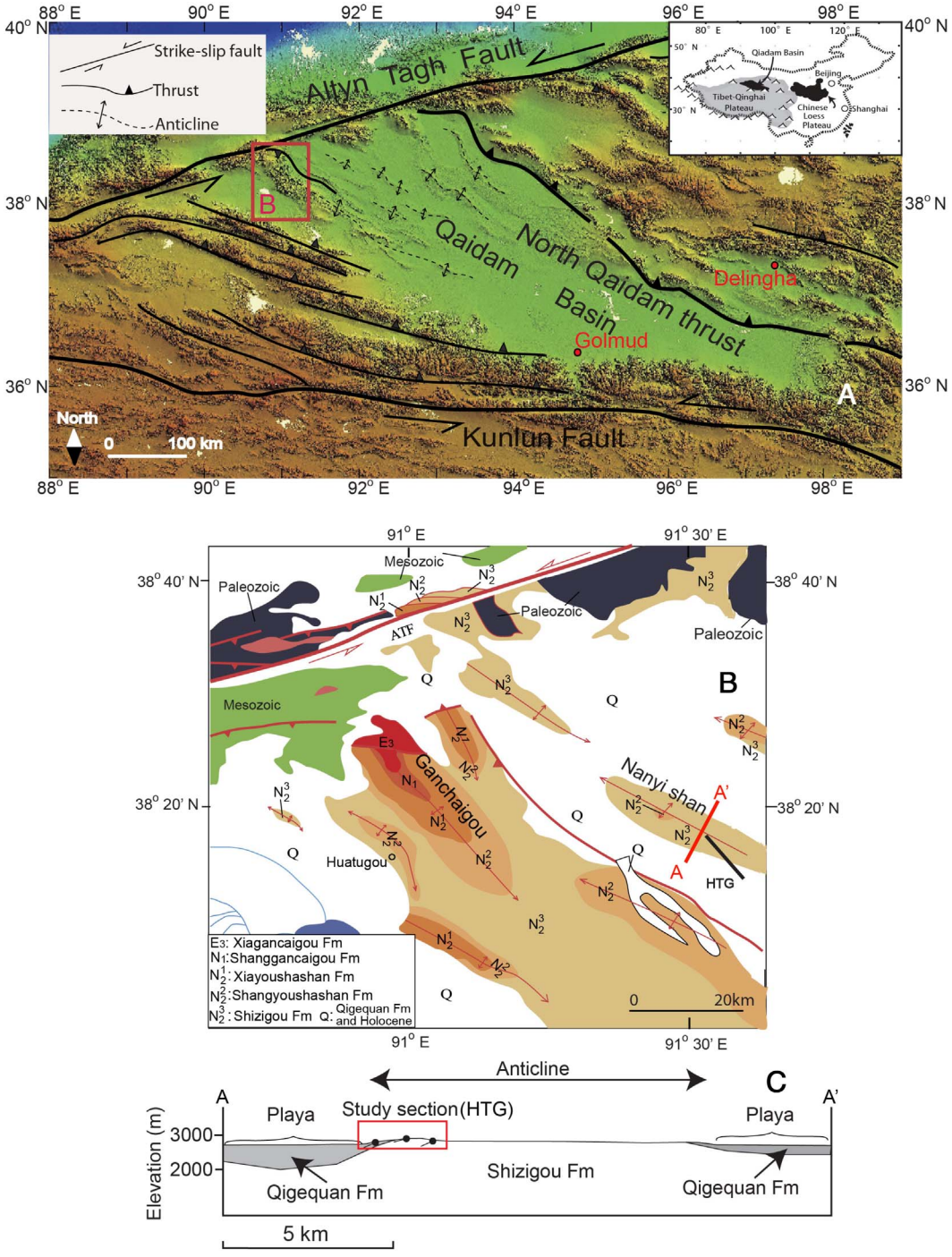

Fig. 1. A: Map of the Qaidam Basin and the location of the study area (based on Yu et al., 2014; Chang et al., 2015). B: Detailed geologic map of the study area and the location of Huatugou section (based on Cai et al., 2012; Y.D. Wang et al., 2012; J.Y. Wang et al., 2012; Chang et al., 2015). C: The cross section of HTG. HTG: Huatugou section.

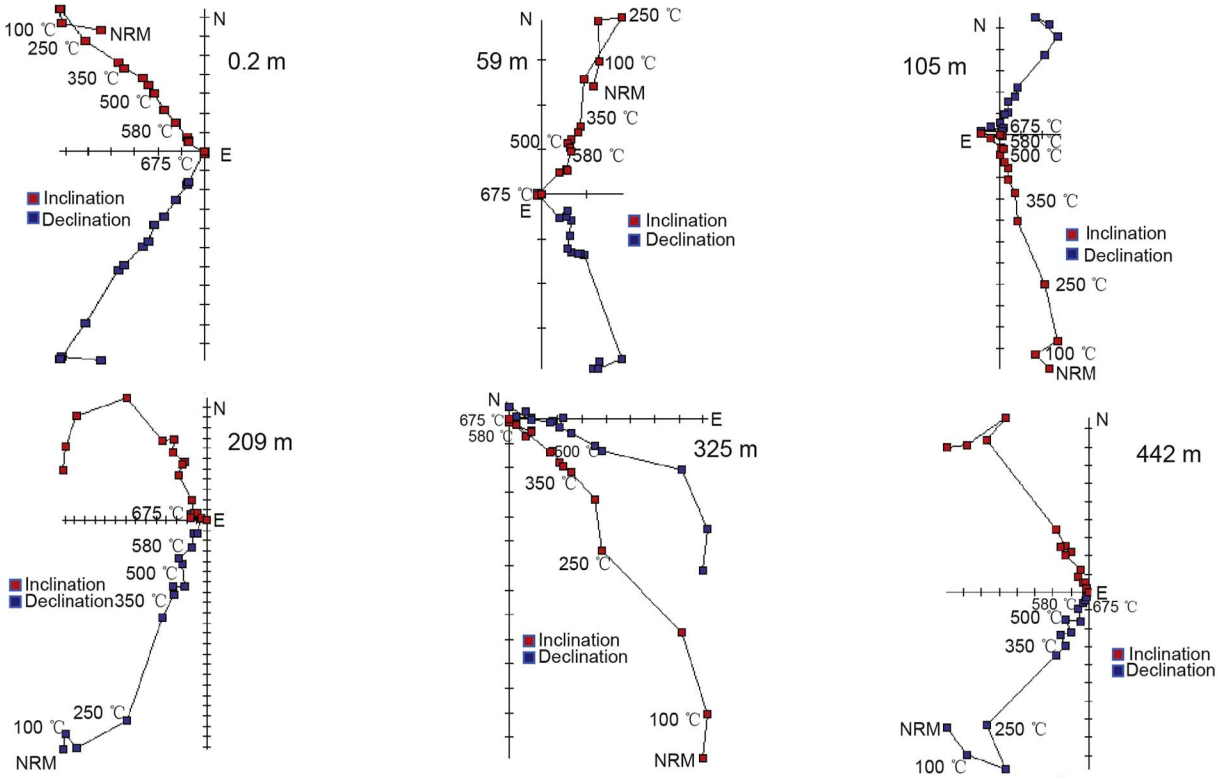

Fig. 2. Orthogonal vector diagrams of representative samples from Huatugou section. The red squares and blue squares represent the vertical and horizontal planes respectively. NRM: natural remanent magnetization. (For interpretation of the references to color in this figure legend, the reader is referred to the web version of this article.)

Quaternary evaporites (e.g., gypsum, carbonate and halite) have been deposited in the western part of the basin (Wang et al., 2013).

The HTG section (from 38°18.16′ N, 91°31.13′ E to 38°15.5′ N, 91°34.2′ E) lies on the southern flank of the Nanyi Shan just east of Ganchaigou anticline in the western Qaidam Basin, with an average elevation of ~2920 m (Fig. 1B). The section includes at least 900-m-thick of strata comprised of the Shizigou Formation and the Qigequan Formation (Fig. 1B and Fig. 1C). However, the upper ~420 m of deposits are covered by salt crust, including ~250 m of strata that are completely covered, so only the lower portion of the section was measured (645 m) and sampled (476 m). The Shizigou Formation in the lower portion of the section is ~375 m thick and characterized by massive siltstone and fine-medium sandstone. The Qigequan Formation is ~270 m thick, and primarily composed of mudstone and conglomerates. The lithology in the HTG section is consistent with those in adjacent areas (e.g., the published Yahu, Lenghu sections and the unpublished QC section) (Fang et al., 2008; Wu et al., 2011; Heermance et al., 2013).

3. Materials and methods

Paleomagnetic samples were taken using a portable gasoline powered core drill, and oriented with a magnetic compass in the field. The sampling interval is about 1 m for the lower 150 m, but changed to be 2–10 m for the interval between 150 and 456 m due to salt cover. In total, 212 paleomagnetic samples were collected from this section. These cylinder samples were cut to a height of ~2 cm and then set for 48 h in a magnetically shielded room before natural remanent magnetization (NRM) was measured. Subsequently, these samples were further subjected to systematic stepwise thermal demagnetization between 100 °C and 675 °C using the MMTD-80 thermal demagnetizer and remanence was measured using the 2G cryogenic magnetometer at the Lanzhou University, China.

Evaporite samples were also collected for geochemical analysis at about 1 m intervals in lower 200-m sediments and 2–10 m for 200–476 m because of partial salt cover. A total of 310 evaporite samples were collected from this section. These samples were ground into fine powder and then examined using an X-ray diffractometer (PANalytical X'Pert Pro MPD diffractometer). The X-ray diffractometer was set with CuKα and Ni filter at a voltage of 40 kV and an intensity of 40 mA. Besides, diffraction patterns were scanned from 3° to 70° with a step size of 0.016711° and a scanning time of 17 min. When all samples finished the examination, the relative content of evaporite minerals was estimated based on X'Pert HighScore software which was produced by PANalytical B.V. This experiment was carried out at the Institute of Earth Environment, Chinese Academy of Sciences, Xi'an, China.

4. Age model determination

Fig. 2 and Fig. 3 show thermal demagnetization diagrams for representative samples. The remanent magnetization of most samples decreased sharply between 250 °C and 300 °C, although some (325 m) show rapid decrease between 100 °C and 150 °C. Accordingly, direction of remanent magnetization shows an apparent change between 250 °C and 300 °C except the sample at 325 m where the variation occurred between 100 °C and 150 °C. The direction of high temperature remanent magnetization steadily goes toward to the origin, indicating that this component is likely characteristic remanent magnetization (ChRM) and the lower temperature component is viscous remanent magnetization (VRM). The remanent magnetization decreases rapidly above 500 °C and above 650 °C for some samples, indicating that magnetite and hematite are the main magnetic minerals carrying remanent magnetization.

In total, 193 samples (91%) yielded stable ChRM directions. The latitude of virtual geomagnetic pole (VGP) is calculated by the declination and inclination obtained from the ChRM of these 193 samples. The observed polarity contains 3 normal and 4 reversed polarity intervals, marked as N1-N3 and R1-R4, respectively (Fig. 4), with N1

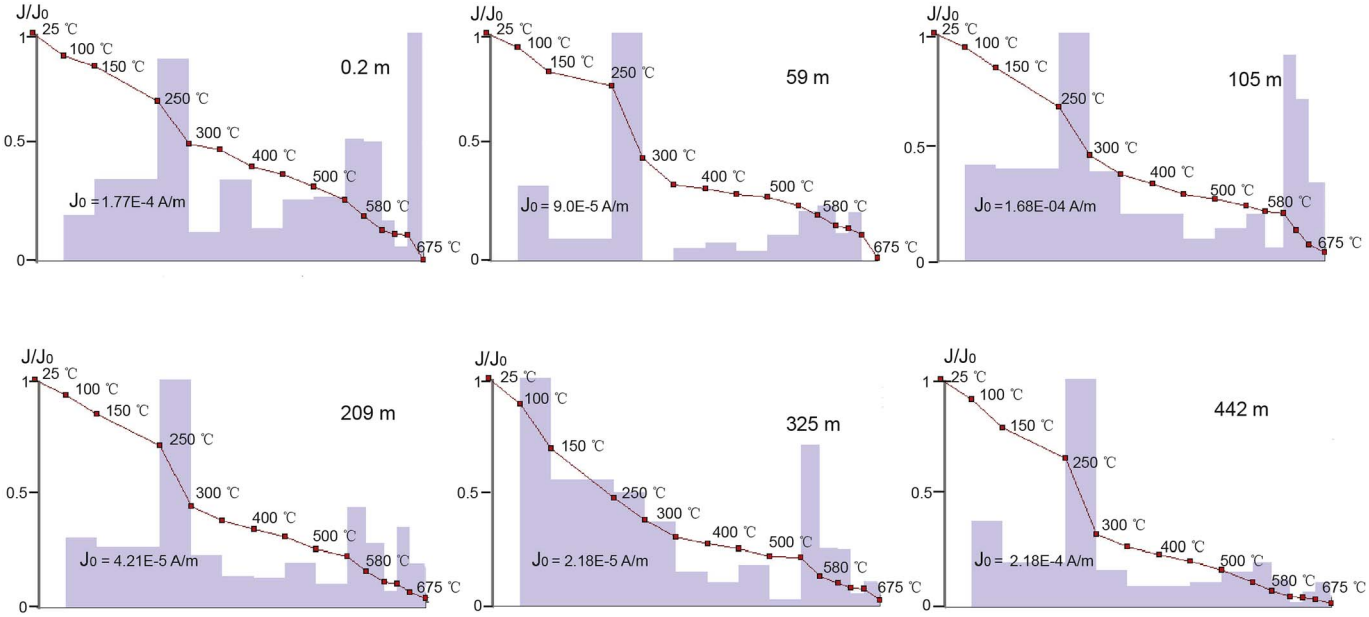

Fig. 3. Attenuation diagrams of the natural remanent magnetization for representative samples from Huatugou section.

significantly longer than N2 but markedly shorter than N3. The geological map of the area shows that this set of strata has a Pliocene-Pleistocene age (Cai et al., 2012; Chang et al., 2015). Based on the duration pattern of N1-N3, N1 to N3 can be well correlated to C2An.3n to C2An.1n. According to this correlation pattern, R4 and R1 (corresponding to C2r and C2Ar) should be significantly longer than R2 and R3 (corresponding to C2An.2r and C2An.1r), consistent with observed data. Thus, the observed polarity can be well-correlated with the Geomagnetic Polarity Time Scale (GPTS) of Gradstein et al. (2012), and we determine the stratigraphic age for the lower 476 m part of the HTG section to be between 3.9 and 2.1 Ma based on piecewise linear interpolation and extrapolation.

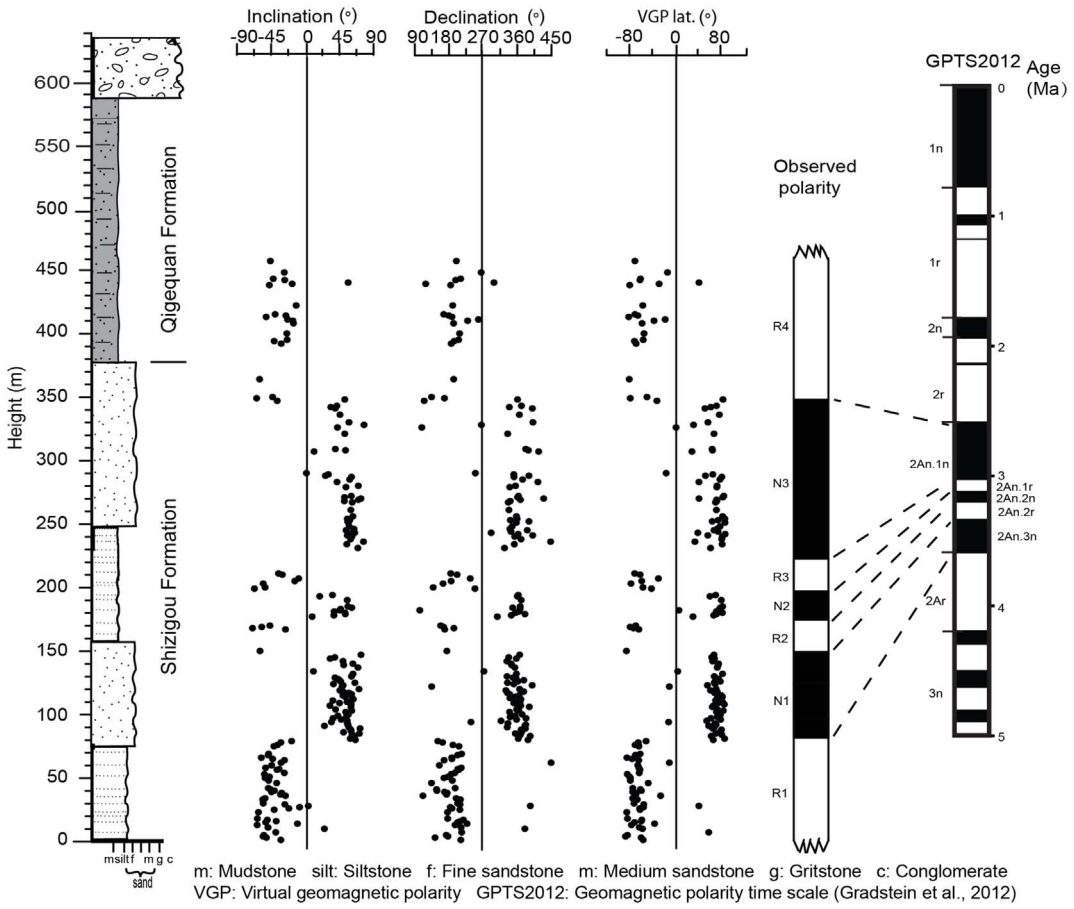

Fig. 4. Age model and lithology of the HTG section in the Qaidam Basin.

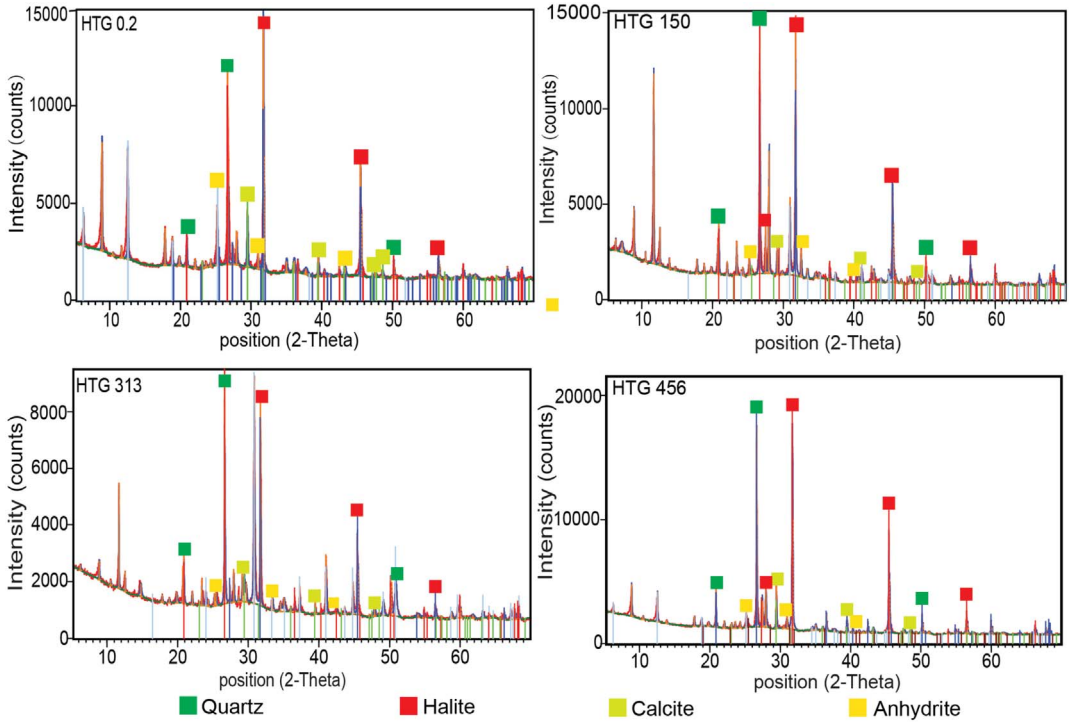

Fig. 5. X-ray diffraction results of representative HTG samples at 0.2, 150, 313, and 456 m (based on Analysis method for clay minerals and ordinary non-clay minerals in sedimentary rocks by the X-ray diffraction, 2010).

5. Evaporite mineral content record

Analysis of X-ray diffractograms reveals the existence of several minerals such as quartz (SiO_2), halite (NaCl), calcite ($CaCO_3$) and anhydrite ($CaSO_4$) (Fig. 5). Fig. 6 shows the relative content variation of these minerals, which was estimated by X'Pert HighScore software. Although the three evaporite mineral records do not show a clear long-term trend, it is clear that the relative content of quartz decreases

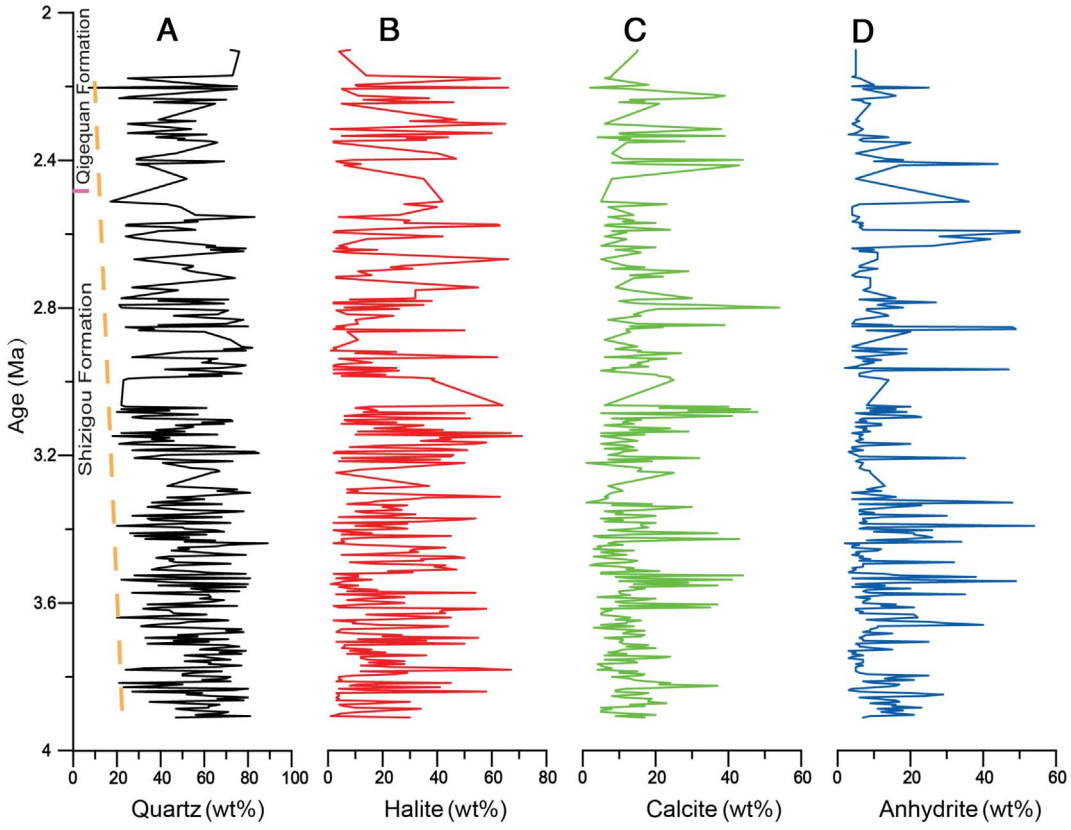

Fig. 6. The content of quartz, halite, calcite and anhydrite in the HTG section versus age.

upsetion (as is shown by the yellow dashed line), indicating an increase in the relative content of evaporite minerals and intensified aridity from 3.9 to 2.1 Ma (Fig. 6).

Our sampling yields a 4-kyr resoluation for the 3.9–3.3 Ma and an average 8-kyr resolution for the 3.3–2.1 Ma. Wavelet analysis reveals that the relative content variation of evaporite minerals is dominated by 100-kyr cyclicity, with a weak contribution from orbital obliquity (41-kyr cyclicity) and precession (23-kyr cyclicity) from 3.9 Ma to 2.1 Ma (Fig. 7). To further study the orbital signals, we performed spectral analysis for evaporite data for the 3.9–3.3 Ma interval, where the sampling resolution is high enough to resolve precession, obliquity, and eccentricity cycles. We focus on the halite record because this record shows large amplitude fluctuations during 3.9–3.1 Ma, whereas the calcite and anhydrite records display smaller amplitude fluctuations and these fluctuations are perturbed by many spikes. 100-, 41-, 23-kyr band cycles are all observed and the 100-kyr cyclicity is stronger than the other two cycles in the halite record (Fig. 8). In addition to these orbital cycles, harmonic cycles like ~60 kyr and ~30 kyr are also observed (Clemens and Tiedemann, 1997; Lu et al., 2004) (Fig. 8). Fig. 9 shows the visual comparison of the 100-kyr band between the halite record and the eccentricity record. It is clear that these two records show some similarities with larger amplitude during 3.6–3.0 Ma and 2.4–2.1 Ma and damped fluctuations between 2.9 and 2.4 Ma.

6. Discussion

6.1. Tectonic timescale variations of inland Asian drying

Quartz and evaporite minerals are the dominant minerals in this stratigraphic succession (Fig. 5). Thus, the decreasing quartz content upsection reveals that the basin has an increasing evaporite mineral content and an intensified drying trend from 3.9 to 2.1 Ma. This observed aridification trend during the Pliocene and early Pleistocene indicated by the evaporite mineral records of the HTG section is also supported by other climatic records from the northwestern China. The sporopollen records from the lacustrine Yahu section in the central Qaidam Basin show that stepwise aridification since Pliocene (especially a widely enhanced aridity at 3.6 Ma) (Wu et al., 2011). The late Miocene to early Pleistocene carbonate content and salt ion records from western Tarim Basin, northwestern China reveal that arid climate has prevailed within the basin since ca. 5.7 Ma (Zhang et al., 2013). The stable hydrogen isotopic composition of leaf-wax *n*-alkanes from the Huaitoutala section in northeastern Qaidam Basin suggest that a dry climate since 4.1 Ma and increasing aridity at 3.1 Ma (Zhuang et al., 2011). In addition, other pollen and geochemical records from the Jiuxi Basin, Linxia Basin, Qaidam Basin and Tarim Basin also show a gradual drying trend since the Pliocene (Ma et al., 2005; Fan et al., 2007; Fang et al., 2008; D.H. Sun et al., 2008; J.M. Sun et al., 2008; Cai et al., 2012; Heermance et al., 2013; Miao et al., 2013).

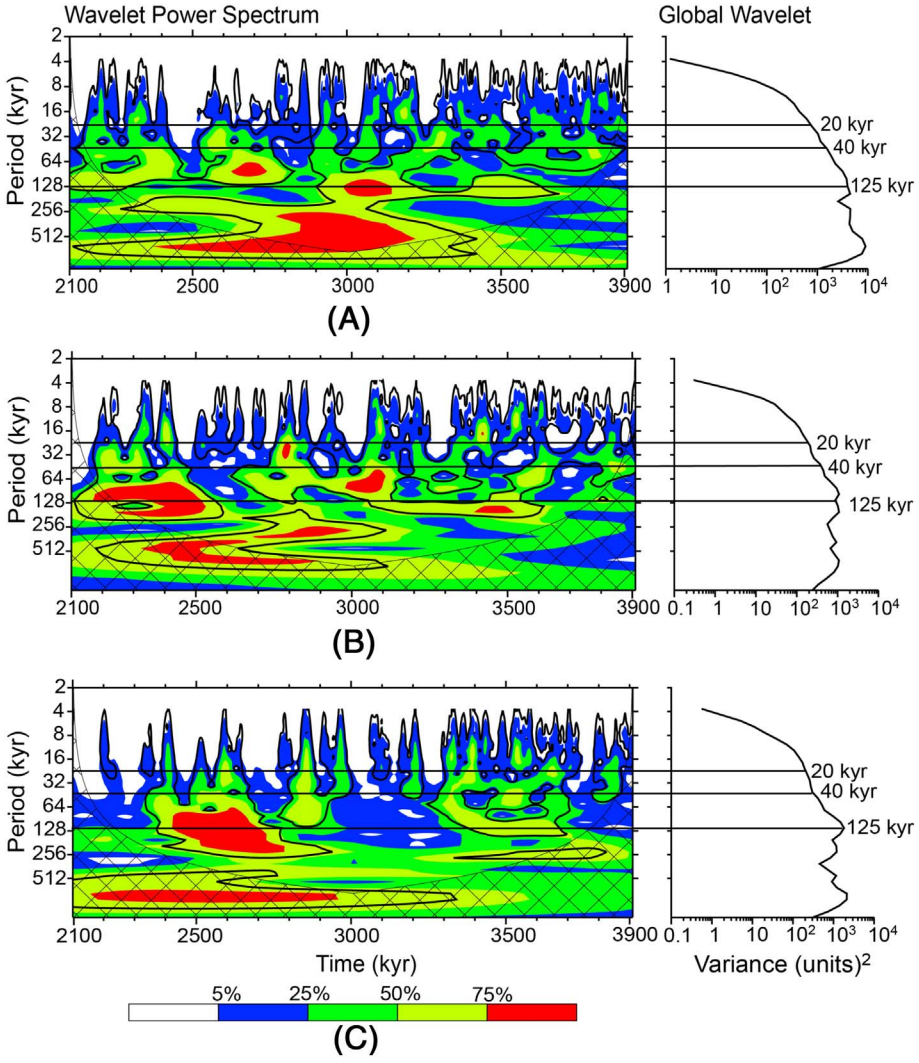

Fig. 7. Wavelet transform (left) (Torrence and Compo, 1998) and the power spectrum (right) of the evaporite mineral records from the HTG section during 3.9–2.1 Ma. (A): halite, (B): calcite, (C): anhydrite. Color scale indicates power, which is scaled to percent total power (warm color indicates larger power). The 125-kyr, 40-kyr, and 20-kyr periodicities are labeled and indicated by the straight black lines. The cross-hatched region is the cone of influence, where zero padding has reduced the variance. The black contour is the 80% significance level, using a red noise background spectrum. (For interpretation of the references to color in this figure legend, the reader is referred to the web version of this article.)

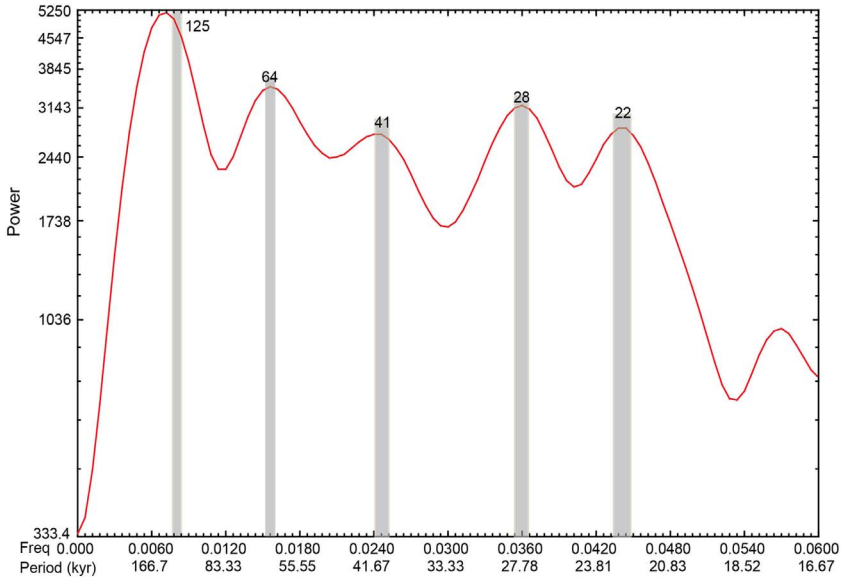

Fig. 8. Spectral density as a function of frequency for the halite record during 3.9–3.3 Ma. The analyses were performed using the Blackman-Tuckey method (Howell et al., 2006). This record was interpolated at 1-kyr intervals.

6.2. Inland Asian drying and insolation forcing

Different from the million year timescale variations, the orbital-timescale Asian aridification history can only be resolved by higher sampling resolution. The smallest periodicity that can be resolved is determined by the Nyquist frequency, half of the sampling rate of a discrete signal system. However, in order to confidently detect the signal, the sampling rate usually needs to be at least 4–5 times larger than the Nyquist frequency. Thus, to detect the precession signal, the appropriate sampling interval needs to be 4 kyr or less. In this record, only the portion of 3.9–3.3 Ma satisfies this requirement with a mean resolution of 4 kyr.

The benthic oxygen isotope records reveal that the ice volume during the Pliocene is dominated by the 41-kyr obliquity signal (Ruddiman et al., 1986; Raymo et al., 2006). By contrast, the halite record during 3.9–3.3 Ma shows that the 100-kyr cyclicity is stronger than the 41-kyr obliquity and 23-kyr precession cyclicity (Fig. 8). It is well known that insolation variations associated with Earth's orbital eccentricity variations are much weaker in comparison with those associated with obliquity and precession (Imbrie et al., 1993). The evaporite mineral records, thus, may show a non-linear response to insolation forcing. Our records are not alone in revealing the particular sensitivity of inland Asian aridity to eccentricity forcing. For example, the late Eocene period gypsum content record from the Xining basin shows apparent 100-kyr cyclicity, attributing to eccentricity forcing (Dupont-Nivet et al., 2007).

There are several possible mechanisms by which the evaporite minerals in inland Asian lakes can enlarge eccentricity forcing. First, the 100-kyr cyclicity could come from a free oscillation internal to Earth's climate system as is proposed by some workers (Nie et al., 2008; Lisiecki, 2010; Nie, 2011; Rial et al., 2013). In this case, the 100-kyr signal is not forced by eccentricity; instead, eccentricity forcing suppresses the 100-kyr signal. Only when the fluctuation amplitude is smaller, the climate system will show enlarged 100-kyr cyclicity. However, Fig. 9 suggests that the 100-kyr-band amplitude variability is similar between the halite content record and eccentricity at some level during 3.9–2.1 Ma, not consistent with prediction of free oscillation forcing. Second, the evaporite mineral records could be controlled by annual insolation instead of summer insolation. Because annual insolation integrates seasonable insolation variation caused by precession, it has more power in eccentricity bands and weak power in precession bands. This could explain the enlarged 100-kyr cyclicity observed here. Alternatively, the weaker 20-kyr and 40-kyr signals might be a bias of age model precision issue. The unevenly sedimentation accumulation rate can weaken the power of the short cycles and enlarge the power of the long eccentricity cycles. Despite this possibility, our data clearly record strong eccentricity-driven climate variability, similar to the results in the Xining Basin (Dupont-Nivet et al., 2007).

7. Conclusions

The evaporite mineral records from the HTG section in the western Qaidam Basin reveal that this part of the basin has been arid since at least 3.9 Ma. At orbital timescales, the evaporite mineral records reveal that paleo-lake evaporation in the Qaidam Basin was particularly sensitive to eccentricity forcing during the Pliocene. Our study provides a good example showing links between the drying of inland Asia and

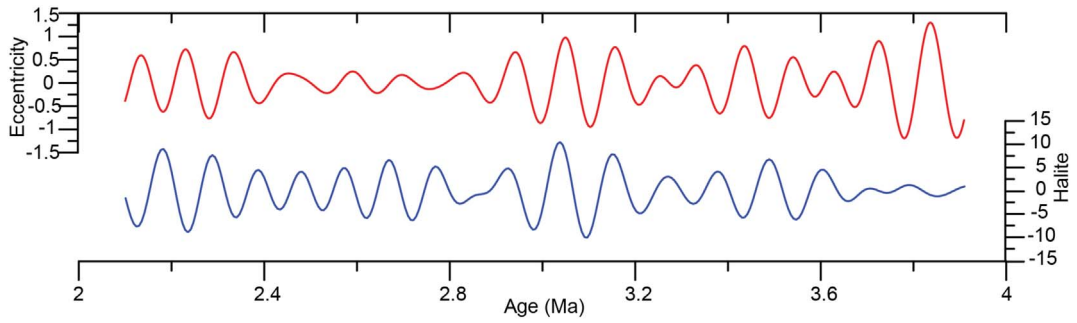

Fig. 9. The filtered 100-kyr band variability associated with halite record and its comparison with the Earth's orbital eccentricity (Laskar et al., 2004).

insolation forcing in the Qaidam Basin, improving understanding of aridification to forcing at orbital timescales.

Acknowledgments

This work was financially supported by the National Key Research and Development Program of China (2016YFE0109500), the (973) National Basic Research Program of China (Grant No. 2013CB956400), the National Natural Science Foundation of China (Grant No. 41422204 & 41672157) to Nie, U.S. National Science Foundation (Grant No. 1348075) to Heermance, and U.S. National Science Foundation (Grant No. 1348005 & 1545859) to Garzione. Many thanks to Ji Shunchuan, Chen Wenhan, Zhang Rui and Gong Lisha for their field assistance. We thank guest editor Prof. H. Hong and two reviewers for comments and T. Herbert for informal discussion.

References

An, Z.S., Kutzbach, J.E., Prell, S.C., 2001. Evolution of Asian monsoons and phased uplift of the Himalaya-Tibetan plateau since late Miocene times. Nature 411, 62–66.

An, Z.S., Zhang, P.Z., Wang, E., Wang, S.M., Qiang, X.K., Li, L., Song, Y.G., Chang, H., Liu, X.D., Zhou, W.J., Liu, W.G., Cao, J.J., Li, X.Q., Shen, J., Liu, Y., Ai, L., 2006. Changes of the monsoon-arid environment in China and growth of the Tibetan plateau since the Miocene. J. Quat. Sci. 26 (5), 678–693 (in Chinese with English abstract).

Cai, M.T., Fang, X.M., Wu, F.L., Miao, Y.F., Appel, E., 2012. Pliocene–Pleistocene stepwise drying of Central Asia: evidence from paleomagnetism and sporopollen record of the deep borehole SG-3 in the western Qaidam Basin, NE Tibetan plateau. Glob. Planet. Chang. 94-95 (94–95), 72–81.

Chang, H., Li, L.Y., Qiang, X.K., Garzione, C.N., Pullen, A., An, Z.S., 2015. Magnetostratigraphy of Cenozoic deposits in the western Qaidam Basin and its implication for the surface uplift of the northeastern margin of the Tibetan plateau. Earth Planet. Sci. Lett. 430, 271–283.

Clemens, S.C., Tiedemann, R., 1997. Eccentricity forcing of Pliocene-early Pleistocene climate revealed in a marine oxygen-isotope record. Nature 385 (6619), 801–804.

Ding, Z.L., Yu, Z., Rutter, N.W., Liu, T., 1994. Towards an orbital time scale for Chinese Loess deposits. Quat. Sci. Rev. 13 (1), 39–70.

Ding, Z.L., Xiong, S.F., Sun, J.M., Yang, S.L., Gu, Z.Y., Liu, T.S., 1999. Pedostratigraphy and paleomagnetism of a ~7.0 Ma eolian Loess–red clay sequence at Lingtai, Loess plateau, north-central China and the implications for paleomonsoon evolution. Palaeogeogr. Palaeoclimatol. Palaeoecol. 152 (1–2), 49–66.

Dregne, H., Kassas, M., Rozanov, B., 1991. A new assessment of the world status of desertification. Desertification Control Bull. 20, 6–18.

Dupont-Nivet, G., Krijgsman, W., Langereis, C.G., Abels, H.A., Dai, S., Fang, X.M., 2007. Tibetan plateau aridification linked to global cooling at the Eocene–Oligocene transition. Nature 445 (7128), 635–638.

Eugater, H.P., Hardie, L.A., 1978. In: Lerman, A. (Ed.), Saline Lakes, Lakes: chemistry, Geology, Physics. Springer-Verlag, New York, pp. 237–293.

Fan, M.J., Dettman, D.L., Song, C.H., Fang, X.M., Garzione, C.N., 2007. Climatic variation in the Linxia basin, NE Tibetan plateau, from 13.1 to 4.3 Ma: the stable isotope record. Palaeogeogr. Palaeoclimatol. Palaeoecol. 247 (3–4), 313–328.

Fang, X.M., Xi, X.X., Li, J.J., Mu, D.F., 1997. The arid events of the late Miocene in the west of China. Chin. Sci. Bull. 42 (23), 2521–2524 (in Chinese with English abstract).

Fang, X.M., Xu, X.H., Song, C.H., Han, W.X., Meng, Q.Q., Torii, M., 2007a. High resolution rock magnetic records of Cenozoic sediments in the Linxia Basin and their implications on drying of Asian inland. J. Quat. Sci. 27 (6), 989–1000 (in Chinese with English abstract).

Fang, X.M., Zhang, W.L., Meng, Q.Q., Gao, J.J., Wang, X.M., King, J., Song, C.H., Dai, S., Miao, Y.F., 2007b. High-resolution magnetostratigraphy of the Neogene Huaitoutala section in the eastern Qaidam Basin on the NE Tibetan plateau, Qinghai Province, China and its implication on tectonic uplift of the NE Tibetan Plateau. Earth Planet. Sci. Lett. 258 (1), 293–306.

Fang, X.M., Wu, F.L., Han, W.X., Wang, Y.D., Zhang, X.Z., Zhang, W.L., 2008. Plio-Pleistocene drying process of Asian inland-sporopollen and salinity records from Yahu section in the central Qaidam Basin. J. Quat. Sci. 28 (5), 874–882 (in Chinese with English abstract).

Feng, S., Fu, Q., 2013. Expansion of global drylands under a warming climate. Atmos. Chem. Phys. 13 (19), 10081–10094.

Gradstein, F.M., Ogg, J.G., Smith, A.G., 2012. The Geologic Time Scale. Cambridge University Press.

Guo, Z.T., Peng, S.Z., Hao, Q.Z., Biscaye, P.E., Liu, T.S., 2001. Origin of the Miocene-Pliocene red-earth formation at Xifeng in northern China and implications for paleoenvironments. Palaeogeogr. Palaeoclimatol. Palaeoecol. 170 (1–2), 11–26.

Guo, Z.T., Ruddiman, W.F., Hao, Q.Z., Wu, H.B., Qiao, Y.S., Zhu, R.X., Peng, S.Z., Wei, J.J., Yuan, B.Y., Liu, T.S., 2002. Onset of Asian desertification by 22 Myr ago inferred from Loess deposits in China. Nature 416 (6877), 159–163.

Hao, Q.Z., Guo, Z.T., 2004. Magnetostratigraphy of a late Miocene–Pliocene loess-soil sequence in the western Loess plateau in China. Geophys. Res. Lett. http://dx.doi.org/10.1029/2003GL019392.

Heermance, R.V., Pullen, A., Kapp, P., Garzione, C.N., Bogue, S., Ding, L., Song, P.P., 2013. Climatic and tectonic controls on sedimentation and erosion during the Pliocene-quaternary in the Qaidam Basin (China). Geol. Soc. Am. Bull. 125 (5–6), 833–856.

Herb, C., Koutsodendris, A., Zhang, W.L., Appel, E., Fang, X.M., Voigt, S., Pross, J., 2015. Late Plio-Pleistocene humidity fluctuations in the western Qaidam Basin (NE Tibetan plateau) revealed by an integrated magnetic–palynological record from lacustrine sediments. Quat. Res. 84 (3), 457–466.

Howell, P., Pisias, N., Ballance, J., Baughman, J., Ochs, L., 2006. Arand Time-Series Analysis Software. Brown University.

Imbrie, J., Berger, A., Boyle, E.A., Clemens, S.C., Duffy, A., Howard, W.R., Kukla, G., Kutzbach, J., Martinson, D.G., McIntyre, A., Mix, A.C., Molfino, B., Morley, J.J., Peterson, L.C., Pisias, N.G., Prell, W.L., Raymo, M.E., Shackleton, N.J., Toggweiler, J.R., 1993. On the structure and origin of major glaciation cycles 2. The 100,000-year cycle. Paleoceanography 8 (6), 699–735.

Laskar, J., Robutel, P., Joutel, F., Gastineau, M., Correia, A.C.M., Levrard, B., 2004. A long term numerical solution for the insolation quantities of the earth. Astron. Astrophys. 428, 261–285.

Li, M.H., Fang, X.M., Yi, C.L., Gao, S.P., Zhang, W.L., Galy, A., 2010. Evaporite minerals and geochemistry of the upper 400 m sediments in a core from the western Qaidam Basin, Tibet. Quat. Int. 218 (1–2), 176–189.

Li, M.H., Fang, X.M., Wang, J.Y., Song, Y.G., Yang, Y.B., Zhang, W.L., Liu, X.M., 2013. Evaporite minerals of the lower 538.5 m sediments in a long core from the western Qaidam Basin, Tibet. Quat. Int. 298 (442), 123–133.

Lisiecki, L.E., 2010. Links between eccentricity forcing and the 100,000-year glacial cycle. Nat. Geosci. 3 (5), 349–352.

Lu, H.Y., Zhang, F.Q., Liu, X.D., 2002. Patterns and frequencies of the East Asian winter monsoon variations during the past million years revealed by wavelet and spectral analyses. Glob. Planet. Chang. 35 (1–2), 67–74.

Lu, H.Y., Zhang, F.Q., Liu, X.D., Duce, R.A., 2004. Periodicities of palaeoclimatic variations recorded by loess-paleosol sequences in China. Quat. Sci. Rev. 23 (18–19), 1891–1900.

Ma, Y.Z., Fang, X.M., Li, J.J., Wu, F.L., Zhang, J., 2005. The vegetation and climate change during Neocene and early quaternary in Jiuxi Basin, China. Sci. China Ser. D Earth Sci. 48 (5), 676–688.

Miao, Y.F., Fang, X.M., Wu, F.L., Cai, M.T., Song, C.H., Meng, Q.Q., Xu, L., 2013. Late Cenozoic continuous aridification in the western Qaidam Basin: evidence from sporopollen records. Clim. Past 9 (4), 1863–1877.

Nie, J.S., 2011. Coupled 100-kyr cycles between 3 and 1 Ma in terrestrial and marine paleoclimatic records. Geochem. Geophys. Geosyst. 12, Q10Z32. http://dx.doi.org/10.1029/2011GC003772.

Nie, J.S., King, J., Fang, X.M., 2008. Late Pliocene-early Pleistocene 100-ka problem. Geophys. Res. Lett. 35, L21606. http://dx.doi.org/10.1029/2008GL035265.

Nie, J.S., Peng, W.B., Möller, Y., Song, Y.G., Stockli, D.F., Stevens, T., Horton, B.K., Liu, S.P., Bird, A.F., Oalmann, J., Gong, H.J., Fang, X.M., 2014. Provenance of the upper Miocene-Pliocene red clay deposits of the Chinese Loess plateau. Earth Planet. Sci. Lett. 407 (407), 35–57.

Nie, J.S., Stevens, T., Rittner, M., Stockli, D., Garzanti, E., Limonta, M., Bird, A., Andò, S., Vermeesch, P., Saylor, J., Lu, H.Y., Breecker, D., Hu, X.F., Liu, S.P., Resentini, A., Vezzoli, G., Peng, W.B., Carter, A., Ji, S.C., Pan, B.T., 2015. Loess plateau storage of northeastern Tibetan plateau-derived Yellow River sediment. Nat. Commun. 6, 8511.

Qiang, X.K., An, Z.S., Song, Y.G., Chang, H., Sun, Y.B., Liu, W.G., Ao, H., Dong, J.B., Fu, C.F., Wu, C., Lu, F.Y., Cai, Y.J., Zhou, W.J., Cao, J.J., Xu, X.W., Ai, L., 2011. New eolian red clay sequence on the western Chinese Loess plateau linked to onset of Asian desertification about 25 Ma ago. Sci. China Ser. D Earth Sci. 54 (1), 136–144.

Raymo, M.E., Lisiecki, L., Nisancioglu, K.H., 2006. Plio-Pleistocene ice volume, Antarctic climate, and the global $\delta^{18}O$ record. Science 313 (5786), 492–495.

Rial, J.A., Oh, J., Reischmann, E., 2013. Synchronization of the climate system to eccentricity forcing and the 100,000-year problem. Nat. Geosci. 6 (4), 289–293.

Ruddiman, W.F., Raymo, M., Mclntyre, A., 1986. Matuyama 41,000-year cycles: North Atlantic Ocean and northern hemisphere ice sheets. Earth Planet. Sci. Lett. 80 (1–2), 117–129.

Song, Y.G., Fang, X.M., Li, J.J., An, Z.S., Miao, X.D., 2001. The late Cenozoic uplift of the Liupan Shan, China. Sci. China Ser. D Earth Sci. 44, 176–184 (supp).

Song, Y.G., Fang, X.M., Torrii, M., Ishikawa, N., Li, J.J., An, Z.S., 2007. Late Neogene rock magnetic record of climatic variation from Chinese eolian sediments related to uplift of the Tibetan plateau. J. Asian Earth Sci. 30 (2), 324–332.

Song, C.H., Hu, S.H., Han, W.X., Zhang, T., Fang, X.M., Gao, J.P., Wu, F.L., 2013. Middle Miocene to earliest Pliocene sedimentological and geochemical records of climate change in the western Qaidam Basin on the NE Tibetan plateau. Palaeogeogr. Palaeoclimatol. Palaeoecol. 395 (2), 67–76.

Stevens, T., Carter, A., Watson, T.P., Vermeesch, P., Lu, H.Y., Andò, S., Garzanti, E., Bird, A.F., Cottam, M.A., Sevastjanova, I., 2013. Genetic linkage between the Yellow River, the Mu Us desert, and the Chinese Loess plateau. Quat. Sci. Rev. 78 (19), 355–368.

Sun, D.H., Liu, D.S., Chen, M.Y., An, Z.S., 1997. Magnetostratigraphy and palaeoclimate of red clay sequences from Chinese loess plateau. Sci. China Ser. D Earth Sci. 40 (4), 337–343.

Sun, Y.B., Clemens, S.C., An, Z.S., Yu, Z.W., 2006. Astronomical timescale and palaeoclimatic implication of stacked 3.6-Myr monsoon records from the Chinese loess plateau. Quat. Sci. Rev. 25 (1–2), 33–48.

Sun, D.H., Su, R.X., Bloemendal, J., Lu, H.Y., 2008. Grain-size and accumulation rate records from late Cenozoic aeolian sequences in northern China: implications for variations in the East Asian winter monsoon and westerly atmospheric circulation. Palaeogeogr. Palaeoclimatol. Palaeoecol. 264 (1–2), 39–53.

Sun, J.M., Zhang, L.Y., Deng, C.L., Zhu, R.X., 2008. Evidence for enhanced aridity in the Tarim Basin of China since 5.3 Ma. Quat. Sci. Rev. 27 (9–10), 1012–1023.

Sun, Y.B., An, Z.S., Clemens, S.C., Bloemendal, J., Vandenberghe, J., 2010. Seven million years of wind and precipitation variability on the Chinese Loess plateau. Earth Planet.

Sci. Lett. 297 (3–4), 525–535.
Torrence, C., Compo, G.P., 1998. A practical guide to wavelet analysis. Bull. Am. Meteorol. Soc. 79, 61–78.
Wang, Y.D., Zheng, J.J., Zhang, W.L., Li, S.Y., Liu, X.W., Yang, X., Liu, Y.H., 2012. Cenozoic uplift of the Tibetan plateau: evidence from the tectonic-sedimentary evolution of the western Qaidam Basin. Geosci. Front. 3 (2), 175–187.
Wang, J.Y., Fang, X.M., Appel, E., Song, C.H., 2012. Pliocene–Pleistocene climate change at the NE Tibetan plateau deduced from lithofacies variation in the drill core SG-1, western Qaidam Basin, China. J. Sediment. Res. 82 (11 − 12), 933–952.
Wang, J.Y., Fang, X.M., Appel, E., Zhang, W.L., 2013. Magnetostratigraphic and radiometric constraints on salt formation in the Qaidam Basin, NE Tibetan plateau. Quat. Sci. Rev. 78 (11), 53–64.
Wang, W.T., Zheng, W.J., Zhang, P.Z., Li, Q., Kirby, E., Yuan, D.Y., Zheng, D.W., Liu, C.C., Wang, Z.C., Zhang, H.P., Pang, J.Z., 2017. Expansion of the Tibetan plateau during the Neogene. Nat. Commun. 8, 15887.
Warren, J.K., 2006. Evaporites: Sediments, Resources and Hydrocarbons. Springer Verlag, Berlin.
Warren, J.K., 2010. Evaporites through time: tectonic, climatic and eustatic controls in marine and nonmarine deposits. Earth Sci. Rev. 98 (3), 217–268.
Williams-Stroud, S.C., Paul, J., 1997. Initiation and growth of gypsum piercement structures in the Zechstein Basin. J. Struct. Geol. 19 (7), 897–907.
Wu, F.L., Fang, X.M., Ma, Y.Z., Mosbrugger, V., Herramnn, M., 2007. Plio-quaternary stepwise drying of Asia: evidence from a 3-Ma pollen record from the Chinese Loess plateau. Earth Planet. Sci. Lett. 257 (1–2), 160–169.
Wu, F.L., Fang, X.M., Herrmann, M., Mosbrugger, V., Miao, Y.F., 2011. Extended drought in the interior of Central Asia since the Pliocene reconstructed from sporopollen records. Glob. Planet. Chang. 76 (1), 16–21.
Xia, W.C., Zhang, N., Yuan, X.P., Fan, L.S., Zhang, B.S., 2001. Cenozoic Qaidam basin, China: a stronger tectonic inversed, extensional rifted basin. Bull. Am. Assoc. Pet. Geol. 85 (4), 715–736.
Yu, X.J., Huang, B.C., Guan, S.W., Fu, S.T., Cheng, F., Cheng, X., Zhang, T., Guo, Z.J., 2014. Anistropy of magnetic susceptibility of Eocene and Miocene sediments in the Qaidam Basin, Northwest Chinese: implication for Cenozoic tectonic transition and depocenter migration. Geochem. Geophys. Geosyst. http://dx.doi.org/10.1002/2014GC005231.
Zhang, Y., Xuan, Z., 1996. Economic evaluation of potassium and magnesium soliddeposit in Kunteyi and Mahai Salt Lake of Qinghai Province. J. Salt Lake Sci. 4 (1), 36–45 (in Chinese with English abstract).
Zhang, Z.G., Han, W.X., Fang, X.M., Song, C.H., Li, X.Y., 2013. Late Miocene–Pleistocene aridification of Asian inland revealed by geochemical records of lacustrine-fan delta sediments from the western Tarim Basin, NW China. Palaeogeogr. Palaeoclimatol. Palaeoecol. 377 (2), 52–61.
Zhuang, G.S., Hourigan, J.K., Koch, P.L., Ritts, B.D., Kent-Corson, M.L., 2011. Isotopic constraints on intensified aridity in Central Asia around 12 Ma. Earth Planet. Sci. Lett. 312 (1–2), 152–163.